University of Stuttgart
Germany

5. Physikalisches Institut

Bachelor Thesis

Setup of a transfer cavity to stabilize a UV optical lattice

Christopher Hendrik Ng

December 1, 2022

Abstract

Frequency stabilisation is a key element to conduct experiments with ultra cold quantum gases. Of special interest in our experiment, is the scan of narrow UV-transitions in dysprosium. To do a sophisticated scan precise frequency control is essential.
In this thesis a transfer cavity is built to stabilize a UV-laser system. The cavity is characterized for 626 nm and 720 nm light. The finesse of the cavity is $\mathcal{F}_{626}$ =754(1),784(1) for p- and s-polarized 626 nm light and $\mathcal{F}_{720}$ =679(1),762(1) for p- and s-polarized 720 nm light.
The cavity will be used as an external reference for frequency stabilisation. Here the cavity will be constantly scanned. From the drift of the peaks a feedback signal can be send to the laser system stabilizing the frequency.

Zusammenfassung

Laser sind der Eckpfeiler jedes modernen Experiments, das sich mit Atomphysik und ultrakalten Quantengasen befasst. Sie können dazu verwendet werden, Atome anzuregen, zu kühlen oder sogar einzufangen. Bei Experimenten mit ultrakalten Quantengasen ist es sehr wichtig, die Laserfrequenz genau kontrollieren zu können. Nach Betrachtung des elektronischen Anregungsspektrums für eine bestimmte Atomspezies, ermöglichen stabile Laserfrequenzen eine gezielte und kontrollierte Abkühlung, sowie das Einfangen von Atomen, welches alles wichtige Schritte für Experimente mit ultrakalten Atomen sind.

Das derzeitige Ziel unserer Forschungsgruppe ist die Realisierung eines Quantengasmikroskops zur Erforschung neuer Materiezustände, die durch die starke magnetische Dipolwechselwirkung zwischen Dysprosiumatomen entstehen. Die Atome werden in ein kurzwelliges (360 nm) optisches Gitter geladen, um die dipolaren Wechselwirkungen zu verstärken.

In dieser Arbeit wird eine Transfer-Cavity aufgebaut und charakterisiert. Dieser Cavity dient als als externe Referenz, um den UV-Laser zu stabilisieren. Der Laser selbst hat inter- interne Referenzen zur Stabilisierung seiner Frequenz, die jedoch durch äußere Einflüsse gestört werden können. Daher kann eine stabile Referenz verwendet werden, um den Laser entsprechend zu korrigieren. In dieser Arbeit ist die Referenz ein 626-nm-Laser, der der durch einen ULE-Resonator (Ultra Low Expansion) stabilisiert wird [1]. Mit dem in dieser Arbeit konstruierten Transferresonator wird das UV-Lasersystem charakterisiert, um den UV-Laser für zukünftige Anwendungen zu stabilisieren.

Die aufgebaute Transfer-Cavity folgt einem Design von Christian Tomschitz[2]. Die Cavity mit einer Gesamtlänge von 18,6(1) cm hat eine eine Finesse von $\mathcal{F}_{626} = 754(1)$ für p-polarisiertes Licht und $\mathcal{F}_{626}$ =784(1) für s-polarisiertes Licht. Für Licht mit einer Wellenlänge von 720 nm wird eine Finesse von $\mathcal{F}_{720} = 679(1)$ für p-polarisiertes Licht und $\mathcal{F}_{720} = 762(1)$ für s-polarisiertes Licht. Außerdem wird die Drift der Cavity gemessen. Der durch Temperaturschwankungen des Resonators verursachte Drift beträgt 8,15(1)GHz/K. Zur Charakterisierung des UV-Lasersystems wird der Drift relativ zum stabilisiertem 626 nm Licht gemessen. Außerdem wird die interne Frequenz-Scan-Funktion charakterisiert. Der Drift des UV-Lasers ist über kurze Zeitspannen klein im Vergleich zum thermischen Drift, den der Resonator erfährt. Die Scanfunktion des Lasers zeigt eine Nichtlinearität [3] sowie einen Unterschied

zwischen dem eingestellten Frequenzabtastabstand und der gemessenen Frequenz-Scan-Distanz. Dieser Unterschied zwischen dem eingestellten Scanbereich und dem gemessenen Scanbereich Bereich kann bis zu 20% betragen.
Zum Zeitpunkt der Erstellung dieser Arbeit können die Messdaten erst nach Abschluss der Messung ausgewertet werden. Ein Ziel für zukünftige Anwendungen ist, die sofortige Auswertung des Drifts im Vergleich zur vorherigen Messung, um ein Steuerungssignal an den Laser zu senden. So kann das Lasersystem über unbestimmte Zeiträume hinweg stabilisiert werden. Bisher wird der Transfer-Resonator nur als Scanning-Resonator verwendet, da die Finesse zu hoch für side-of-fringe locking ist. Um die Cavity auf den ULE-stabilisierten 626 nm Laser zu locken muss ein PDH-Signal erzeugt werden. Hierzu könnte das auf dem Red pitaya basierende Lock programm einer anderen Arbeitsgruppe aus unserem Intitut verwendet werden.
Zur Charakterisierung des UV-Lasersystems ist eine komplexere Abstandsmessung zwischen dem stabilisierten 626-nm-Laser und dem 720-nm-Laser erforderlich. Dies würde eine genaue Untersuchung der Nichtlinearität in der Scanfunktion sowie der Drift des des 720-nm-Lichts ermöglichen. Außerdem müssen Langzeitdriftmessungen des 720-nm-Lasers durchgeführt werden, um die Auswirkungen deutlicher erkennen zu können.

Introduction

Lasers are the cornerstone of every modern experiment involving atomic physics and ultra cold quantum gases. They can be used to excite, cool or even trap atoms.
In ultra cold quantum gas experiments it is very important to have precise control over the laser frequency. After considering the electronic excitation spectrum for a particular atomic species, stable laser frequencies allow targeted and controlled cooling and trapping of atoms, important steps for experiments with ultra cold atoms to explore new phases of matter.
The current goal of our research group is to realize a quantum gas microscopes to explore new states of matter that arise due to the strong magnetic dipole interaction between dysprosium atoms. The atoms will be loaded into a short wavelength (360 nm) optical lattice to enhance the dipolar interactions.
In this thesis a transfer cavity is set up and characterized. This cavity will serve as an external reference in order to stabilize the UV-laser. The laser itself has internal references to stabilize its frequency, but these can be subject to drifts through perturbation from outside influences. Therefore, a stable reference can be used to correct the laser accordingly. In the thesis the reference is a 626 nm laser, that is stabilized by an ultra low expansion (ULE) cavity [1].
Using the transfer cavity constructed in this thesis, the UV-laser system is characterized, in order to stabilize the UV-laser for future applications.

Eidesstattliche Erklärung

Hiermit erkläre ich, dass ich diese Arbeit selbstständig verfasst habe, dass ich keine anderen als die angegebenen Quellen verwendet habe und dass jegliches wörtlich oder sinngemäß übernommenenes Material als solches gekennzeichnet wurde. Die eingereichte Arbeit ist weder vollständig noch in wesentlichen Teilen Gegenstand eines anderen Prüfungsverfahrens gewesen. Das elektronische Exemplar stimmt mit den anderen Exemplaren überein.

Stuttgart, December 1, 2022 Christopher Hendrik Ng

Contents

Introduction **3**

1 Gaussian optics **13**
1.1 Paraxial wave equation . . . 13
1.2 Gaussian beam . . . 15
1.3 Resonator theory . . . 17

2 Self-built transfer cavity **23**
2.1 Construction and setup of the cavity . . . 23
2.2 Characterization of the cavity . . . 25
2.2.1 Initial measurements of the cavity . . . 25
2.2.2 Modematching . . . 27
2.2.3 Set-up and characterization using 626 nm . . . 29
2.2.4 Set-up and characterization for 720 nm . . . 33
2.2.5 Degenerate modes and asymmetric peaks . . . 35
2.2.6 Drift of the cavity . . . 37
2.3 Summary . . . 41

3 Characterization of the UV-system **43**
3.1 Introduction . . . 43
3.2 Characterization of the 720 nm laser . . . 43
3.3 Summary . . . 45

4 Conclusion **47**

Bibliography **48**

Acknowledgments **51**

5 Appendix **53**

1 Gaussian optics

When trying to create a model that describes the propagation of light, it is very important to consider the wave and particle behavior of light. Where a particle model holds the benefit of describing a precise propagation over long distances it lacks the capability to describe phenomena like interference. These can only be explained by treating light as a wave and not a particle. The foundation of the wave description is the Huygens' principle. Which states that each point of a wave front is the origin of a spherical wavelet [4]. Ideally, a description of light combines both of those properties.

1.1 Paraxial wave equation

The Maxwell equations describe the behavior of the electromagnetic fields [5].

$$\vec{\nabla} \cdot \vec{\mathbf{E}} = \rho \tag{1.1}$$

$$\vec{\nabla} \cdot \vec{\mathrm{B}} = 0 \tag{1.2}$$

$$\vec{\nabla} \times \vec{\mathrm{E}} = -\frac{\partial \vec{\mathbf{B}}}{\partial t} \tag{1.3}$$

$$\vec{\nabla} \times \vec{\mathrm{B}} = \mu_0 \vec{\mathbf{j}} + \mu_0 \epsilon_0 \frac{\partial \vec{\mathbf{B}}}{\partial t} \tag{1.4}$$

Here $\vec{\mathbf{E}}$ is the electric field, $\vec{\mathbf{B}}$ is the magnetic field, ρ is the electric charge density and $\vec{\mathbf{j}}$ is the electric current density. In a vacuum both ρ and $\vec{\mathbf{j}}$ are zero due to the absence of charge carrying particles. Using the Maxwell Faraday equation the behavior for propagation for an electromagnetic wave is derived by applying the rotation operator to both side of the equation.

$$\nabla \times \vec{\nabla} \times \vec{\mathbf{E}} = \nabla \times -\frac{\partial \vec{\mathbf{B}}}{\partial \mathrm{t}} \tag{1.5}$$

Using the identity rot(rot $\vec{\mathbf{F}}$) = grad(div$\vec{\mathbf{F}}$)-$\Delta\vec{\mathbf{F}}$ equation (1.5) can be written as

$$\frac{\partial^2 \vec{\mathbf{E}}}{\partial t^2} - \Delta\vec{\mathbf{E}} = 0 \tag{1.6}$$

This is equation is also know as the *wave equation.* The two most common solutions are the plane and the spherical wave. The plane wave is described by

$$\vec{\mathbf{E}}(\vec{\mathrm{r}}, \mathrm{t}) = \mathrm{E}_0 \exp(i(\vec{\mathbf{k}} \cdot \vec{\mathbf{r}} - \omega\mathrm{t})). \tag{1.7}$$

The wave travels in the direction of the $\vec{\mathbf{k}}$-vector. E_0 is the amplitude and ω is a phase. At any given time the surfaces joining all points of equal phase are known as wave fronts [4]. The envelope of the wave stays constant over time and is independent of distance traveled. The spherical wave on the other hand, has a time dependent envelope and propagates in all directions. It is described by

$$\vec{\mathbf{E}}(\vec{\mathrm{r}}, \mathrm{t}) = \frac{\mathrm{E}_0}{r} \exp i(\vec{\mathrm{k}} \cdot \vec{\mathrm{r}}). \tag{1.8}$$

Looking at the solutions of the wave equation both approaches seem to contradict each other. Both describe observed behavior of a wave. Moving forward the general idea is to find a solution where the nature of the plane wave is conserved while only adding a slightly time dependent envelope. As a consequence of the requirement that the beam envelope only changes slowly over traveled distance is that the wave front encloses a small angle to the optical axis. The position and time dependant solution for such a wave is given by

$$\vec{\mathbf{E}}(\vec{\mathrm{r}}, \mathrm{t}) = \vec{\mathbf{A}}(\vec{\mathbf{r}}) \cdot \exp\left(-i\vec{\mathbf{k}} \cdot \vec{\mathbf{r}}\right) \cdot \exp\left(i\omega t\right) \tag{1.9}$$

Here $\vec{\mathbf{A}}(\vec{\mathbf{r}})$ is the envelope function of the beam, where A(r) slowly changes over time. Considering the wave equation

$$\left(\vec{\nabla}^2 - \frac{1}{c^2}\frac{\partial^2}{\partial t^2}\right) u(\vec{r}, t) = 0 \tag{1.10}$$

the spacial and temporal components of the wave function $u(\vec{r}, t)$ can be separated.

$$u(\vec{r}, t) = A(\vec{r})T(t) \tag{1.11}$$

Substituting the separated form and simplifying it,

$$\frac{\vec{\nabla}^2 A}{A} = \frac{1}{c^2 T}\frac{d^2 T}{dt^2} \tag{1.12}$$

is obtained. These partial differential equations are solved.

$$\frac{\vec{\nabla}^2 A}{A} = -k^2 \tag{1.13}$$

$$\frac{1}{c^2 T}\frac{d^2 T}{dt^2} = -k^2 \tag{1.14}$$

Without loss of generality the time dependence is eliminated and the Helmholtz equation is obtained.

$$\vec{\nabla}^2 A + k^2 A = 0 \tag{1.15}$$

When implementing the solution given in equation (1.9) in the Helmholtz equation (1.15)

$$\Delta\vec{\mathbf{E}} + \vec{k}^2\vec{\mathbf{E}} = 0 \tag{1.16}$$

and applying the transverse Laplace operator this equation turns into

$$\Delta_t\vec{\mathbf{A}} - 2ik\frac{\partial}{\partial t}\vec{\mathbf{A}} = 0. \tag{1.17}$$

This is known as *transverse wave equation*.

1.2 Gaussian beam

One possible solution to the transverse wave equation given in equation (1.17) is the Gaussian beam [4].

$$\vec{\mathbf{E}}(\vec{r}, t) = E_0\frac{w_0}{w(z)}\exp\frac{-r^2}{w(z)^2}\exp\left(-i\left(kz + k\frac{r^2}{2R(z)}\right)\right) \tag{1.18}$$

Here E_0 is the Amplitude of the electric field. Furthermore r is the radial distance to the center of the beam, z is the distance from the beam waist in direction of propagation. The beam width is given by $w(z)$, where the minimal beam width is described by w_0, also called waist w_0, and k is the wave number. The Gaussian beam gets its name from the intensity profile in direction of propagation. Here the intensity profile is given by a Gaussian distribution. A schematic of the Gaussian beam is depicted in figure 1.1

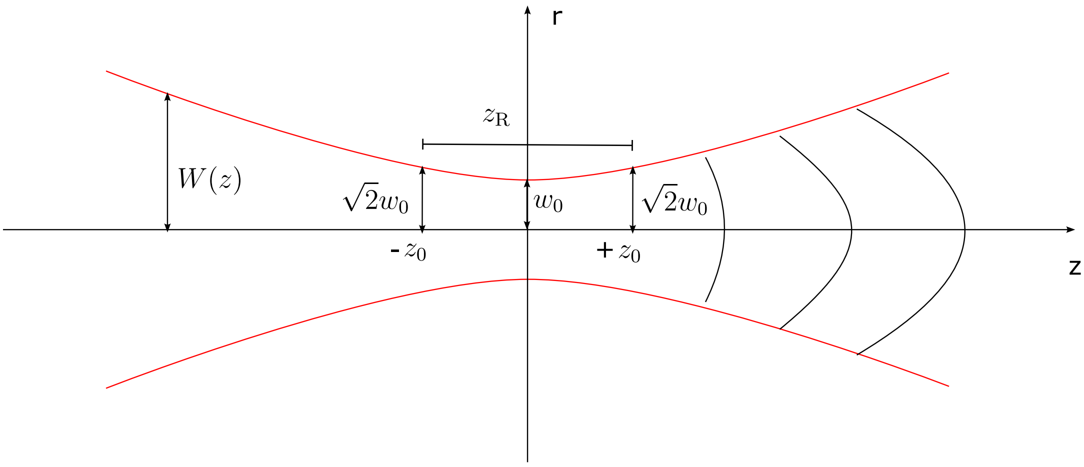

Figure 1.1: This Figure depicts a schematic of a Gaussian beam. From $-z_0$ to z_0 the beam can be approximated as a plane wave. This range until the beam width w(z) reaches $\sqrt{2}w_0$ is called Rayleigh length z_R. The curvature of the wave front increases with the distance z from the beam waist z_0.

In a short range around the beam width minimum, the beam can be approximated as a collimated beam. This approximation is valid until the beam waist has grown to $\sqrt{2}\mathrm{w}_0$. The range from -z_0 to $+z_0$ is called Rayleigh length z_R and is calculated by

$$\mathrm{z_R} = \frac{\pi \cdot \mathrm{w}_0^2}{\lambda}. \tag{1.19}$$

The Curvature of the wavefront increases with distance to the beam waist z. By using

$$R(z) = z\left[1 + \left(\frac{z_R}{z}\right)^2\right] \tag{1.20}$$

the curvature can be calculated. Similar to the curvature the width of the beam is also dependant on z. The evolution of the beam width with increasing distance z to the beam waist w_0 is given by

$$w(z) = w_0\sqrt{1 + (\frac{z}{z_R})^2}. \tag{1.21}$$

1.3 Resonator theory

A optical resonator is a widely used tool in experimental physics. Some examples are reference cavities, spectrum analyzers and resonators surrounding the gain medium in lasers . The first is the most interesting for this thesis. The basis for a reference cavity is the Fabry-Perot interferometer (FPI). Here two mirrors with curvature R_1,R_2, the reflectivities $\mathcal{R}_1$ and $\mathcal{R}_2$ are placed in a distance L apart from each other. In the cavity the light can interfere destructively or constructively. When constructive interference occurs the intensity of the light increases greatly. Due to the increased intensity more light is transmitted through the cavity. This is called a transmission peak. A sketch of a Fabry-Perot interferometer is given in figure 1.2.

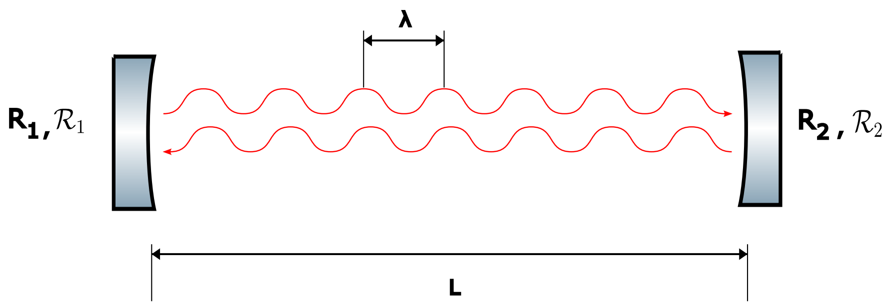

Figure 1.2: This figure depicts a sketch of two mirrors with the radii R_1, R_2, the reflectivity $\mathcal{R}_1$, $\mathcal{R}_2$ and the distance L in between the mirrors .

Resonance occurs when the distance L is a multiple of $\lambda/2$. So for

$$\frac{\lambda}{2} \cdot n = L \ , n \in \mathbb{N} \tag{1.22}$$

the interference of the light with itself results in a standing wave.
The radii and reflectivity of the mirrors define the most important characteristics of the resonator the free spectral range ν_{FSR} and the Finesse $\mathcal{F}$. Following the condition given in equation (1.22) the free spectral range (FSR) is given by the distance between two standing waves (Intensity maxima) . Utilizing that the wavelength λ can be written as $\lambda = c \cdot \nu$ The frequency position of a standing wave in dependence of n is expressed by

$$\nu_n = \frac{n \cdot c}{2L}. \tag{1.23}$$

When determining the FSR the position of two adjacent maxima are subtracted from each other. The FSR is calculated by

$$\nu_{\mathrm{FSR}} = \frac{c}{2L}. \tag{1.24}$$

The FSR is only one of the defining characteristics of the cavity. The finesse $\mathcal{F}$ describes how sharp the transmission peaks of the cavity are. Using formula (1.25)

$$\mathcal{F} = \frac{\nu_{\text{FSR}}}{\text{FWHM}} \tag{1.25}$$

the finesse is calculated. The finesse is not only a measure of sharpness for transmission peaks but it also describes how many times the light is reflected on average before transmission. The finesse scales with the reflectivity of mirrors used. For mirrors with the same reflectivity the Finesse is calculated by

$$\mathcal{F} = \frac{\pi\sqrt{\mathcal{R}}}{1-\mathcal{R}} \quad \text{, where } \mathcal{R} = \sqrt{\mathcal{R}_1\mathcal{R}_2}. \tag{1.26}$$

If the mirrors have different reflectivities $\mathcal{R}_1$ and $\mathcal{R}_2$ the reflectivity $\mathcal{R}$ is given by $\mathcal{R} = \sqrt{\mathcal{R}_1\mathcal{R}_2}$. This also affects the intensity of the transmitted light. The transmitted Intensity is determined by

$$I_{\text{T}} = I_0 \left[1 + \left(\frac{2\mathcal{F}}{\pi}\right)^2 \sin^2\left(\frac{\nu\pi}{\Delta\nu_{\text{FSR}}}\right)\right]^{-1} \tag{1.27}$$

A detailed derivation of the expression given in formula (1.27) is given in [6]. The intensity of the transmitted light is distributed in a Lorentzian line shape. Due to line-broadening caused by outside perturbation a Voight profile is observed. Figure 1.3 shows the effect of different finesses on the transmission peaks. With increasing finesse, the width of the peak decreases and the amplitude increases.

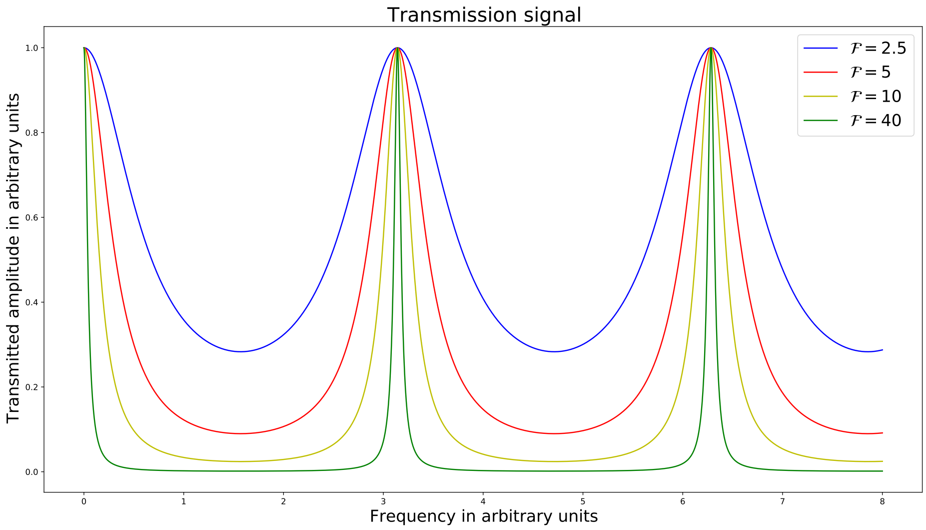

Figure 1.3: This figure depicts the line shape of transmission peaks for the same cavity with different finesses. The higher the finesse, the sharper are the peaks.

Another important factor to consider when constructing a cavity is the stability. A standing wave in a FPI cavity is only possible in Gaussian optics when the stability condition is satisfied. From ray transfer matrix calculations [7] the stability condition is defined as

$$0 \leq g_1 g_2 \leq 1. \tag{1.28}$$

Here g_1 and g_2 are defined as $g_i = 1 - \frac{L}{R_i},\ i \ \epsilon \ [1, 2]$, where L is the length of the resonator and R_1 and R_2 are the radii of the mirrors. This condition is depicted in figure 1.4 for several different builds of FPI.

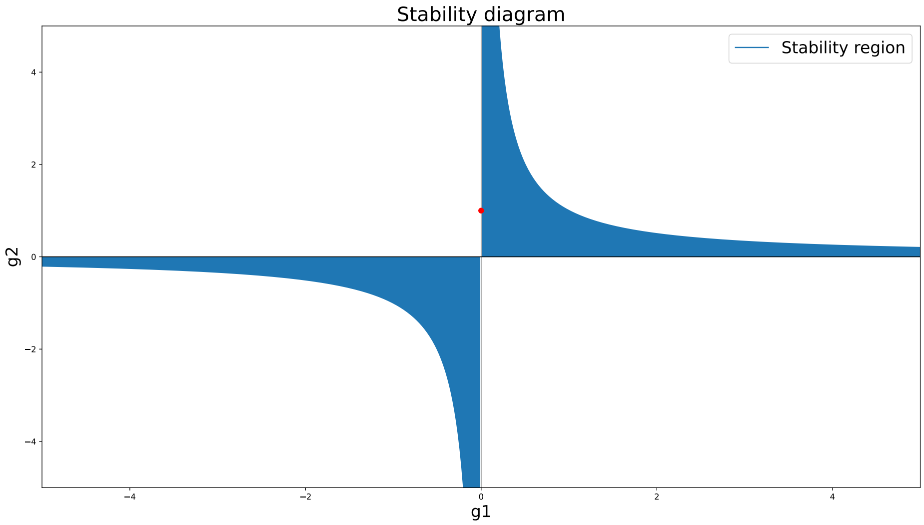

Figure 1.4: This figure depicts the stability condition over the parameters g_1 and g_2 for an optical resonators. If g_1 and g_2 are within the blue area the cavity is stable. The red dot marks the position of the constructed cavity in this diagram.

So far only one case of incoming light has been discussed. In the so called fundamental mode there is no additional phase difference upon reflection and the incoming beam has been reflected directly back at itself. However there are resonant modes that project the beam back on itself after multiple reflections. These are called higher order modes. Higher order modes can be expressed in the basis of Laguerre-polynomials or Hermite-polynomials. The basis is chosen by considering the symmetry of the cavity. In case of radial symmetry along the axis of propagation Laguerre-Gaussian modes can occur. These modes ring shaped modes show radial symmetry with multiple rings of high intensity around a central peak. If the cavity doesn't have radial symmetry, Hermite-Gaussian modes can occur. The pattern of Hermite-Gaussian modes is axial-symmetric.
The constructed cavity is cylindrical so radial symmetry is given. In the case of higher order modes occurring, these modes could be described in the Laguerre-polynomial basis. A plot of Lagurre-Gaussian modes is shown in figure 1.5.

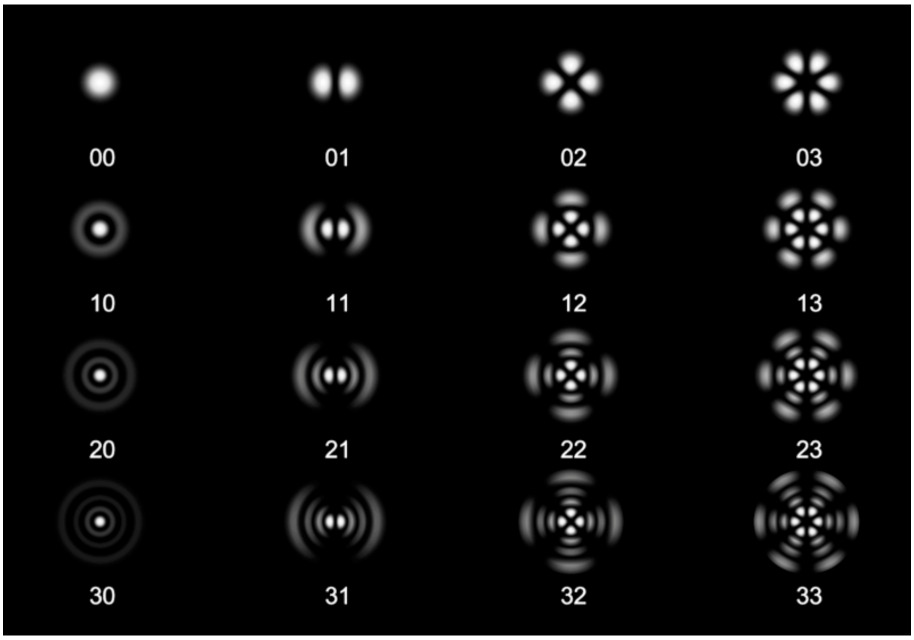

Figure 1.5: This figure shows different Laguerre-Gaussian modes depending on the indices p and l [8]. The (0,0)-mode is the fundamental mode. The higher order modes show symmetries because the beam is reflected multiple times until it is fully reflected back upon itself.

A more detailed description and a derivation of the Laguerre-Gaussian mode is given in [9].

2 Self-built transfer cavity

2.1 Construction and setup of the cavity

The cavity design is based on a design from Christian Tomschitz described in [2]. The advantage of this design is that many off-the-shelf parts are used and parts are readily available. The cavity utilizes two different mirrors, a plane and a concave mirror. The plane mirror is mounted on a Piezo crystal to control the length L of the cavity. The length of the cavity is measured from the reflective surface of one mirror to the reflective surface of the second mirror. These mirrors, including the plane mirror with the Piezo, are mounted on mirror holders with a metal tube, the so called *spacer*, in between them. This way a constant distance between the two mirror holders is ensured.
A 3D model of the cavity is sketched in figure 2.1.

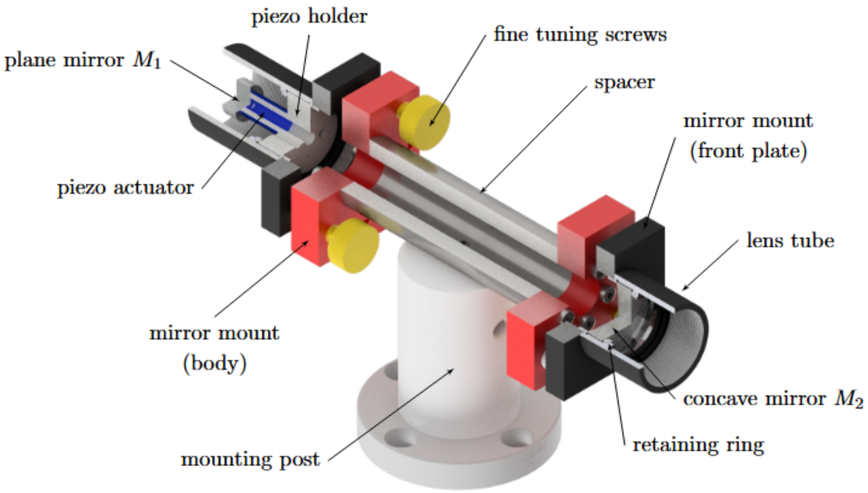

Figure 2.1: This figure depicts a quarter-cut of the cavity. The cavity is mounted on a mounting post. The mirrors are held by mirror holders screwed to a metallic spacer. The concave mirror is positioned in a lens tube. The plane mirror is glued to a cylindrical Piezo actuator. This Piezo is glued to a metal holder plate that fits into a lens tube [2].

This design is called a hemispherical resonator. The used concave mirror is a Thorlabs CM254-100-E02 400-750 nm backside polished mirror. The used plane mirror is an Edmund optics #87-368 with a diameter of 12.5 mm and a 400-750 nm dielectric broadband coating with a polished backside. The Piezo is PICMA P-080.341 with a travel distance of $11(2)\mu$m. The spacer as well as the Piezo-holder are custom designed parts. The sketches of the spacer and the Piezo-holder can be found in the appendix.

2.2 Characterization of the cavity

2.2.1 Initial measurements of the cavity

Before constructing the cavity, the properties of each part are measured independently to ensure that the constructed cavity fulfills our demands. First the reflectivity of the mirrors is measured to determine the expected finesse $\mathcal{F}$. Since the quality of the dielectric coating varies between mirrors, even if they are produced in the same coating run, multiple mirrors of the same type are ordered and tested. The cavity needs to perform well for 626 nm and 720 nm light. Furthermore, the reflectivity is also polarisation dependent. To measure the reflectivity laser light of 626 nm is shone upon the mirror. The incident intensity and the transmitted intensity are measured with a THORLABS PM100A power meter. Using a polarising beam splitter (PBS) and a $\frac{\lambda}{2}$-plate the power and polarisation of the incoming light is adjusted. A sketch of the measurement is depicted in figure 2.2.

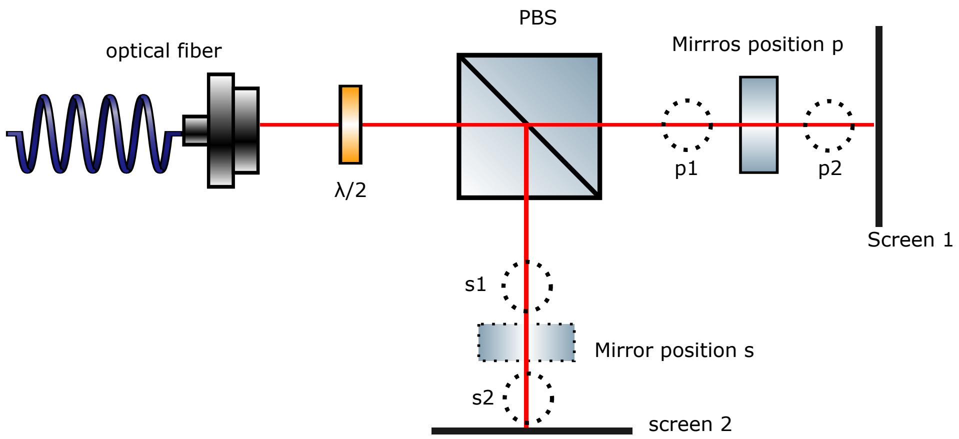

Figure 2.2: This figure shows a sketch of the experimental setup to measure the reflectivity with an angle of incidence 0°. The light transmitted through the PBS is p-polarised and the reflected light is s-polarised. At the positions s1 and p1 the incoming intensity is measured. Where at the positions s2 and p2 the transmitted intensity is measured by a powermeter.

Following equation (1.26), the mirrors with the highest reflectivity for the wavelengths of 626 nm and 720 nm in both s- and p-polarisation are chosen to achieve the highest possible finesse. The cavity will be a scanning cavity. Constantly scanning the cavity allows real-time drift measurement. This yields the benefit of a higher resolution compared a locked cavity that is limited by the FSR. For the plane mirror the measured reflectivity for s-polarised 626 nm light is 99.94(5)% and 99.80(5)% for p-polarised light. The measured reflectivities for the chosen concave mirror are 99.98(5)% for p-polarised light and 99.96(5)% for s-polarised light with a wave length of 626 nm.
These measurements are used to calculate the finesse of the cavity with these mirrors. For p-polarised light the finesse is calculated to

$$\mathcal{F}_p = \frac{\pi\sqrt{\mathcal{R}_p}}{1-\mathcal{R}_p} \approx 5000(2000) \text{ , with } \mathcal{R} = \sqrt{\mathcal{R}_1\mathcal{R}_2}. \tag{2.1}$$

For s-polarised light, the finesse is calculated to $\mathcal{F}_s \approx 6000(2000)$. The error for this measurement is very high even assuming an uncertainty of 0.05%, because as seen in formula (1.26), the finesse diverges as the reflectivity $\mathcal{R}$ approaches 1. Due to the high reflectiviy of the used mirrors the estimated error also diverges. The finesse calculated from the reflectivity measurements is depicted in table 2.1, whereas the measured reflectivities are listed in table 5.1.

Table 2.1: This table lists the finesse calculated from the measured reflectitvities for 626 nm and 720 nm light depending on the polarisation of the incoming light. The data used for the relfectivities is recorded in tab5.1.

wavelength in nm	polarisation	finesse
626	p	5000(2000)
626	s	6000(2000)
720	p	5000(2000)
720	s	6000(2000)

Apart from the finesse the stability condition for the utilized mirrors needs to be met in order to set the distance L between the mirrors. For hemispheric cavities one mirror curvature is infinitely large because of the plane mirror. So the stability condition is only dependent on the curvature of the second mirror. As described in equation (1.28) the g-factors are given by $g_i = 1 - \frac{L}{R_i},\ i \,\epsilon\, [1, 2]$, plugging in a curvature radius of 20 cm for the concave mirror. The stability condition can be written as

$$0 \leq 1 \cdot \left(\underbrace{1 - \frac{L}{R_2}}_{g_2} \right) \leq 1 \tag{2.2}$$

Here g_1 is equal to 1 since $R_1 = \infty$. Solving the condition for L results in a range of stable lengths L is calculated to

$$L \leq R_2 = 20 \text{ cm}. \tag{2.3}$$

For distances shorter than 20 cm the cavity fulfills the stability condition. To ensure that the cavity stays at a length that fulfills the stability condition whilst still having a high FSR a spacer length of 10 cm is chosen. Additionally to this spacer length, the width of the mirror mounts and the distance from the mirror mounts to the mirrors have to be taken into account. These are measured to 8.6 cm with an uncertainty of 0.1 cm. This adds up to a total length of L =18.6(1) cm. The error in length of the spacer is negligible when compared to the error of the mirror holders, since the spacer is industrially manufactured. Knowing the cavity length its FSR is calculated as described by formula (1.24).

$$FSR = \frac{c}{2 * L} = \frac{c}{2 * 0.186(1) \text{ m}} = 805.9(1) \text{ MHz} \tag{2.4}$$

The transfer cavity has a FSR of 805.9(1) MHz.

2.2.2 Modematching

The goal of modematching is to optimize the resonance for the ground mode and in turn maximize the transmitted intensity. Therefore, the mode of the incoming beam should match the resonator mode as good as possible in its curvature. As discussed in the section about Gaussian optics, the curvature of the beam in equation 1.20 is dependent on the Rayleigh length and the distance from the waist. In the hemispheric design chosen for this cavity, the beam waist is situated on the inside of the plane mirror. So in this case, the distance z from the waist is equal to the distance in between the two mirrors L.

$$R(z) = z + \frac{z_R}{z} = L + \frac{z_R}{L} = R_2 \tag{2.5}$$

Here $R(z)$ is the wavefront curvature which should be equal to the curvature of the concave mirror R_2. When inserting equation (1.19) into equation (2.5) and solving it for w_0, the beam waist for optimal modematching can be calculated.

$$w_1 = \sqrt{\frac{\lambda}{\pi} \sqrt{L R_2 - L^2}} \tag{2.6}$$

For a wavelength λ of 626 nm, a Length L of 18.6 cm and a mirror curvature of 20 cm the calculated beam waist $w_1 = 101\ \mu$m.
To focus the beam down to the desired waist inside the cavity, a coupling lens needs to be chosen. The focal length can be calculated by using equation (2.7). A detailed derivation of this formula is given in [2].

$$f = \pi \frac{w_0 w_1}{\lambda} \tag{2.7}$$

The beam coming out of the optical fiber has a waist of $\approx 800\ \mu$m. When focusing the beam down to the calculated waist of $w_1 = 101\ \mu$m a lens with a focal length of 40.5 cm is needed. There is no readily available lens with a focal length of f =40.5 cm. Instead a THORLABS AC254-400-B is used. This achromatic lens has a focal length of 40 cm and a broadband dielectric coating from 400 nm to 750 nm. Since the focal length differs from the calculated optimum, the resulting modematching is worsened.
Since the 720 nm and 626 nm light both need to be coupled into the cavity through the same lens, the beam width of the incoming 720 nm light needs to be chosen accordingly to couple into the cavity. To achieve a wavefront curvature matching the mirror the beam needs a waist of 108 μm. Solving equation 2.7 for w_0 and using the calculated focal length of 40.5 cm, w_0 is found to be 860 μm.
Modematching is not only important when dealing with resonators, but also when coupling light in and out of optical fibers. As discussed above, since both wavelengths use the same lens to couple into the cavity the 720 nm light requires a certain waist to match the cavity mode as well as possible. Light coming out of a fiber diverges strongly. A lens of the right focal length can be used in front of the fiber to have a collimated beam with a desired waist. The beam waist is calculated using

$$f = \frac{\pi}{4} \frac{\Phi_{\mathrm{MFD}} D}{\lambda} \tag{2.8}$$

Here Φ_{MFD} is the mode field diameter of the fiber. D is the diameter of the beam behind the lens of focal length f if the fiber is placed in the lens focus. λ is the wavelength of the light. The mode field diameter Φ_{MFD} of the optical fiber is 4.5 μm. With a desired waist of 108 μm, the focal length of the outcoupling lens is calculated to f= 8.44 mm using formula (2.8).

2.2.3 Set-up and characterization using 626 nm

The cavity uses a frequency stabilized 626 nm laser as a reference. As a first step the 626 nm light needs to be coupled into the cavity. To achieve this, the 626 nm light is guided to the coupling lens and focused into the cavity through an optical setup shown in figure 2.3. The beam waist is measured at the focus position. Here a slight ellipticity is measured. On the large axis the beam has a waist of 102(1) μm and a waist of 93(1) μm. This differs from the beam width calculated in section 2.2.2. Therefore, modematching worsens which can lead to higher oder modes.

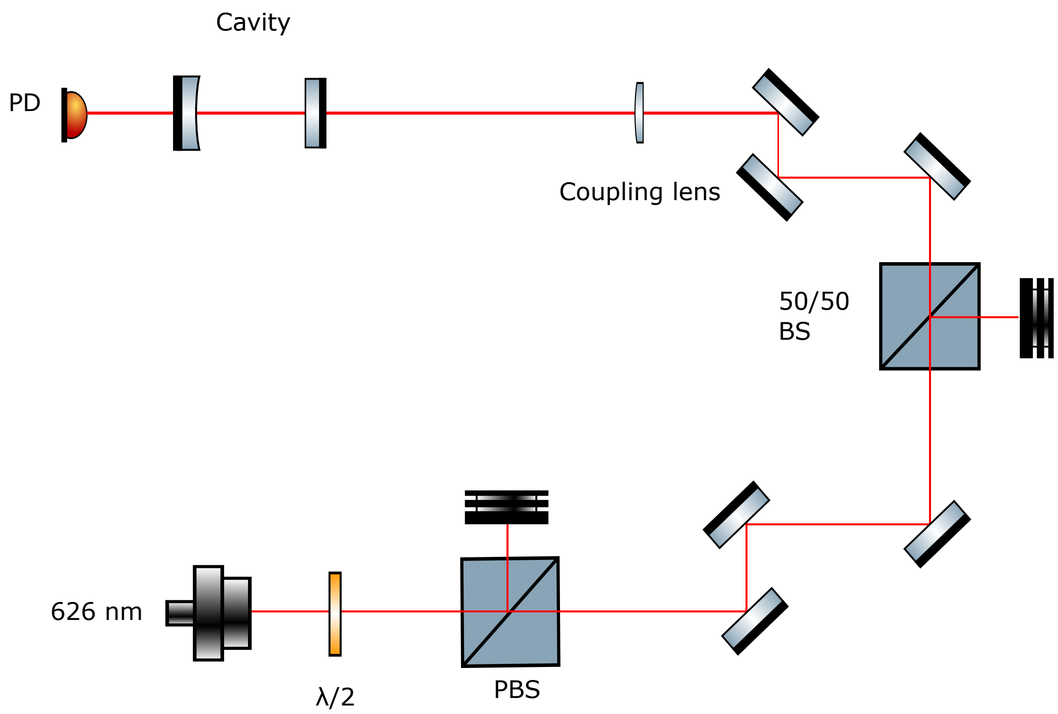

Figure 2.3: This figure shows a sketch of the experimental set up used to couple the 626 nm light into the cavity and observe it. A photo diode used to detect the transmission of the cavity. Where as 'BS' and 'PBS' denote beam splitter and polarizing beam splitter respectively.

Here the $\frac{\lambda}{2}$ plate in combination with the PBS is used to adjust the incoming intensity. The 50/50 BS will become important when the 720 nm light will be coupled into the cavity. The two mirrors right in front of the coupling lens are utilized to center the incoming beam on the lens. The incoupling lens itself is mounted on THORLABS SM1V10 as well as a THORLABS LM1XY(/M) to optimize the lens position in all 3 dimensions for maximum coupling efficiency. The

THORALBS SM1V10, enables fine adjustment of the coupling lens along the optical axis. Meanwhile the THORLABS LM1XY allows precise adjustment perpendicular to the optical axis to ensure that the lens is hit in the center. The photodiode itself is a THORLABS PDA36A-EC switchable gain photodiode with a wavelength selective filter in front of the sensor. The filter is a THORLABS FBH630-10. The incoupling lens is a THORLABS AC254-400-B.
When everything is properly aligned and the 626 nm light is coupled into the cavity and an alternating triangle signal is applied to the Piezo transmission peaks are visible when viewing the output of the photdiode. By measuring the distance between two different peaks of the same order and the width of individual peaks, FSR and finesse of the cavity can be calculated.
To identify peaks of the fundamental mode, the resonance condition is utilized. The Piezo can extend its length by 11(2) μm over a voltage range of 120 V. This results in an approximate adjustment of $\Delta L = 91.5$ nm/V. Using the resonance condition given in equation (1.22), the Piezo has to move half a wave length from one resonance peak for the cavity to be resonant again. So if the peaks are 3.4(7) V apart from each other on the scanning signal, they are most likely of the same order. In case of degenerate modes this assumption doesn't hold up. More information on degenerate modes is given in the subsection on degenerate modes.
In figure 2.4 and figure 2.5, the intensity of the transmitted light is shown. From the data in these plots the FSR as well as the FWHM of the transmission peaks are calculated. The lower amplitude peaks seen in figure 2.4 are most likely higher order modes. Since their amplitude is less than half of the fundamental mode and their position is not in close proximity to the fundamental mode these higher order modes don't cause any problems for the measurement.

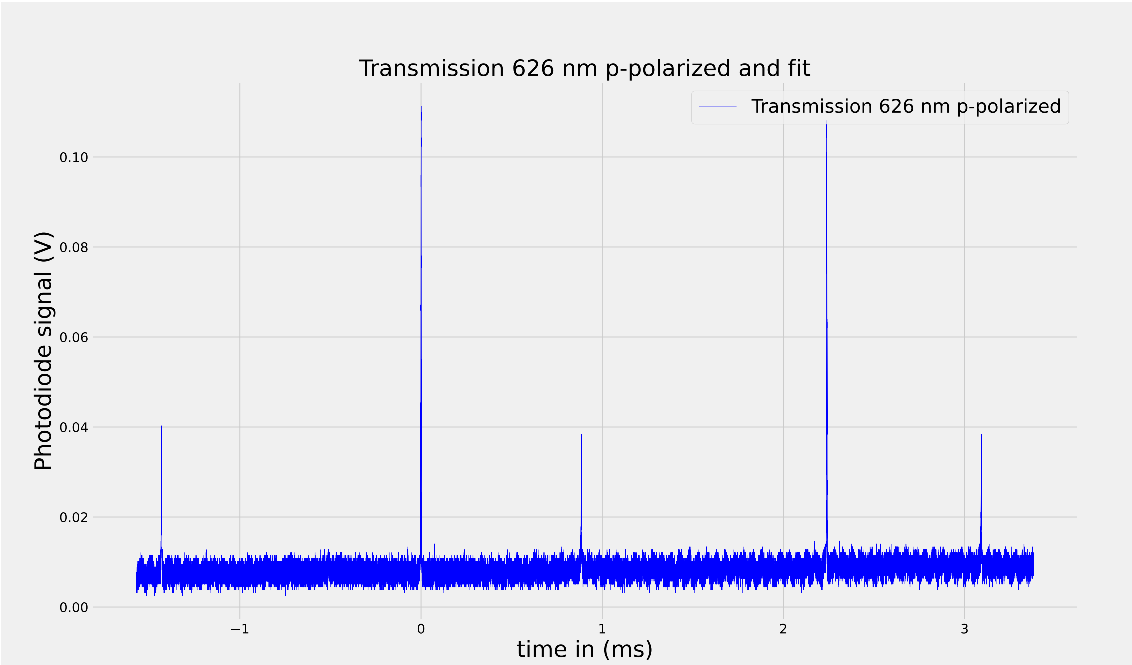

Figure 2.4: This figure shows the transmission signal of the cavity, recorded at a wavelength of 626 nm, a scanning frequency of 50 Hz and a scan amplitude of 4 V_{pp}. Here the two largest observed peaks are the fundamental mode peaks. By measuring the distance between the two peaks the FSR of 2.372(1) ms is determined.

A FSR of 2.372(1) ms is measured. To determine the FWHM of the transmission peaks the scope is triggered on a falling flank of the fundamental mode peaks and the recorded time window is reduced to achieve a higher resolution of a single peak. After recording the data a Gaussian curve is fitted to the signal. A Gaussian curve and its fit are depicted in figure 2.5. For the fit a Gaussian function is used:

$$f(x) = a \cdot \exp\left(-\frac{(x-x_0)^2}{2\sigma^2}\right). \tag{2.9}$$

When defining the Gaussian function like this the FWHM is defined as FWHM $= 2\sqrt{2\ln 2}\sigma$.

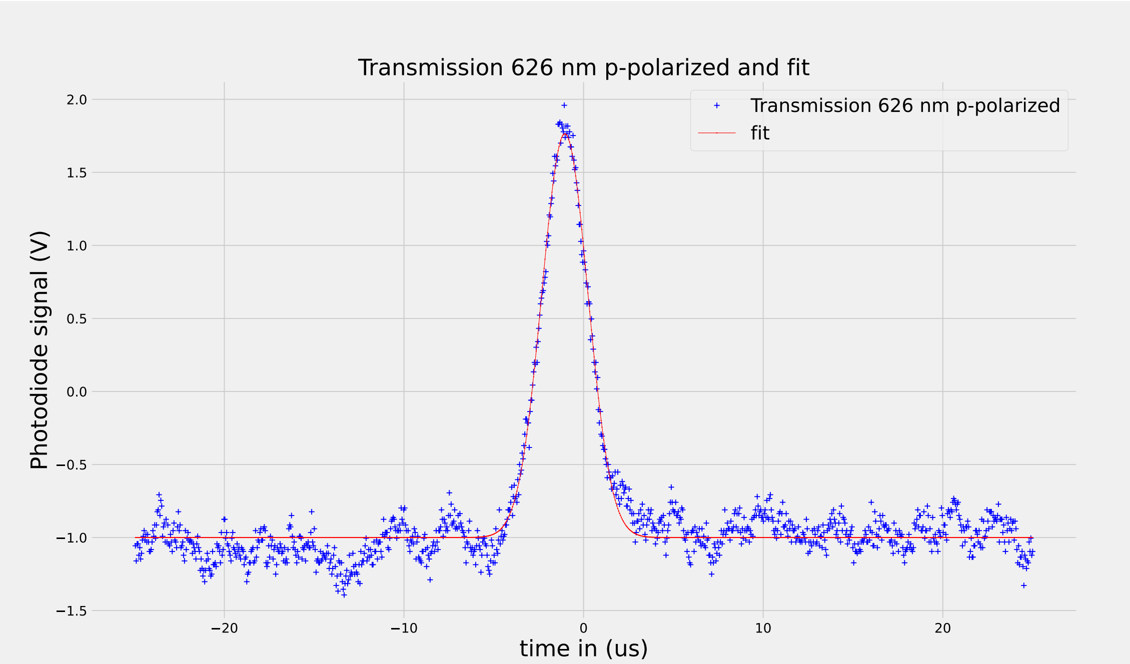

Figure 2.5: This figure shows a close up of a single ground order transmission peak for p-polarized 626 nm light. A Gaussian curve is fitted to the data to determine the FWHM. A FWHM of 3.143(1) μs is calculated.

With the fitted data a FWHM of 3.143(1) μs is calculated. It is very important to note that the scan frequency has to stay the same over the measurement of the FSR and FWHM. If the scan frequency is altered in between measurements the calculated finesse wouldn't be without a unit of measurement. This is then plugged into formula (1.25) a finesse of 754 is calculated for p-polarized 626 nm light.

$$\mathcal{F}_p = \frac{FSR}{FWHM} = \frac{2.372(1)\ \text{ms}}{3.143(1)\ \mu\text{s}} = 754(1) \tag{2.10}$$

This measurement is repeated for s-polarized light. The finesse is calculated to $\mathcal{F}_s = 784(1)$. All measured and calculated parameters (FSR, FWHM, $\mathcal{F}$) are listed in table 5.2.
Comparing these results to the ones that were calculated in section 2.2.1 a big difference is observed. The results being this different can originate from not perfect modematching and the imprecise measurement of reflectivity.

2.2.4 Set-up and characterization for 720 nm

To couple 720 nm light into the cavity, the experimental setup shown in figure 2.3 needs to be expanded by another optical arm. The explicit additions are shown in figure 2.6.

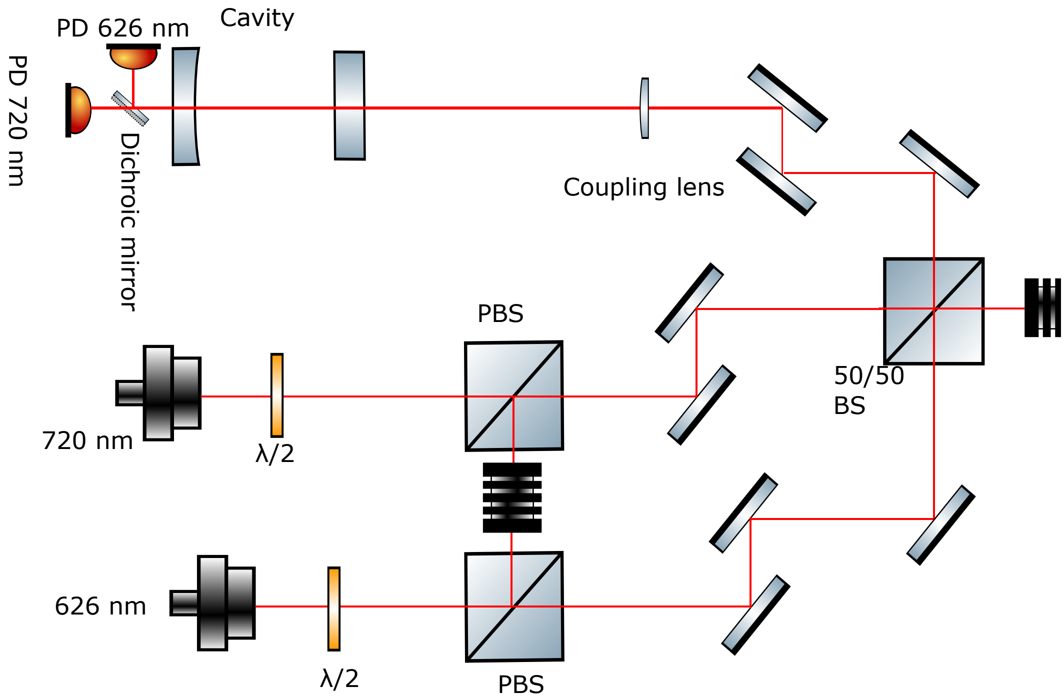

Figure 2.6: This figure shows a sketch of the optical set up used to couple both 626 nm and 720 nm light into the cavity. The base layout of the 720 nm arm is identical to the 626 nm arm until both paths unite at the BS. Behind the cavity a dichroic mirror is placed to separate the transmission by wavelength. The 720 nm is transmitted and 626 nm is reflected. Each transmission signal is measured by its own photodiode.

The dichoric mirror THORLABS DMLP 650 is a and the photodiode to detect the 720 nm light is the THORLABS PDA36A-EC. The photdiode detecting 626 nm is a THORLABS PDA100A-E.
Similar to chapter 2.2.3 the FSR and FWHM of the 720 nm light are measured to determine the finesse of the cavity. Fitting the FWHM for s-polarized 720 nm light results a FWHM of 3.129(1) μs. A graph of the peak as well as the fit are shown in

figure 2.7. With a measured FSR of 2.514(1) ms, the finesse is calculated to 762.

$$\mathcal{F}_s = \frac{FSR}{FWHM} = \frac{2.514(1)\ \mathrm{ms}}{3.129(1)\ \mu\mathrm{s}} = 762(1) \tag{2.11}$$

The same measurement is conducted for 720 nm p-polarized light, $\mathcal{F}_p = 679(1)$. A plot of the transmission signal used to determine the FSR of 2.51 ms is depicted in figure 2.8.

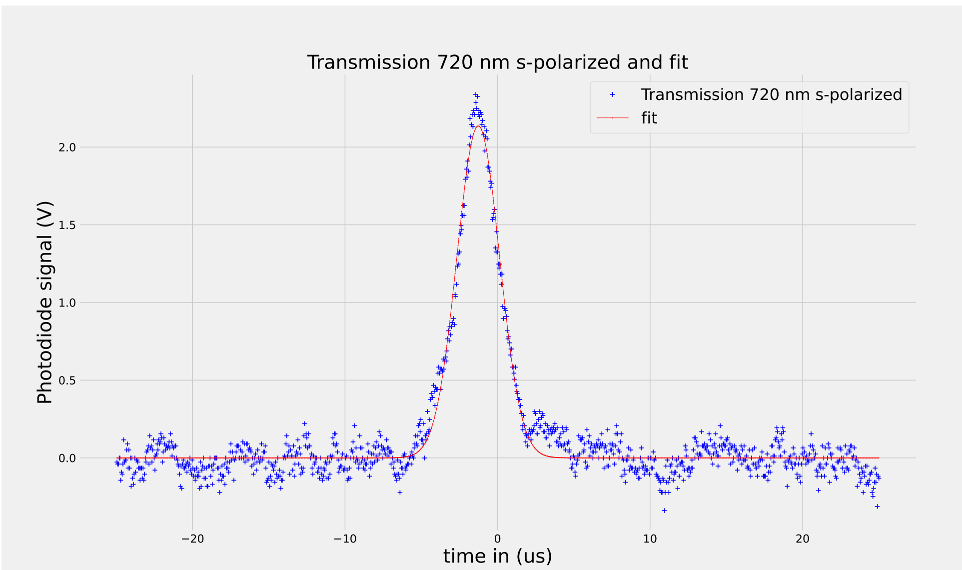

Figure 2.7: This figure shows a close up of a single ground order transmission peak for s-polarized 720 nm light. A Gaussian curve is fitted to the data to determine the FWHM. From the fit a FWHM of 3.129(1) μs is calculated.

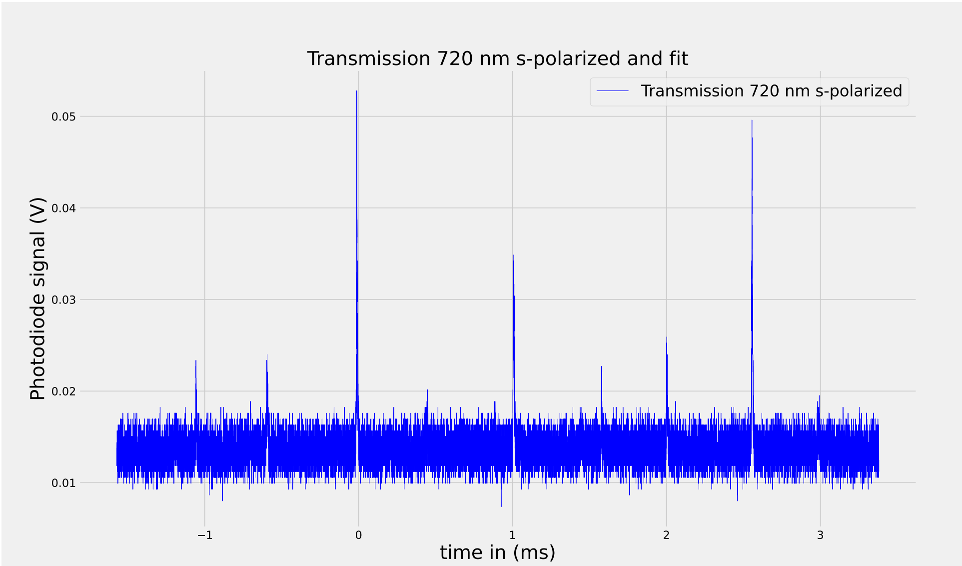

Figure 2.8: This figure shows the transmission signal of the cavity, recorded at a wavelength of 720 nm, a scanning frequency of 50 Hz and a scan amplitude of 4 V_{pp}. Here the two largest observed peaks are the ground order peaks. By measuring the distance between the two peaks the FSR is found to be 2.514(1) ms.

Similar to the FSR measurement for 626 nm light higher order modes are observed for 720 nm light as well. In figure 2.8 three higher order modes are observed in between two fundamental mode peaks. The higher order mode peak with about amplitude of the fundamental mode peak will become a challenge later on, since it might mess with peak detection. The only option to avoid this problem is to recouple both lasers into the cavity.

2.2.5 Degenerate modes and asymmetric peaks

A particular challenge that can be encountered when constructing an optical resonator includes degenerate Modes. Optical modes are degenerate modes when multiple modes with different parameters has the same energy. In a first attempt the cavity was set up with a total length of L =19.6 cm. At this length degenerate modes appeared in the 626 nm light.
These modes are spatially close together which makes the identification of the fundamental modes peaks very difficult. Due to the close proximity of the peaks to each other mode identification using a CCD camera is not possible. To avoid this problem the original spacer is shortened by 1 cm from 11 cm to 10 cm, resulting in a total cavity length of 18.6(1) cm. A picture is taken and depicted in figure 2.9 of the

degenerate modes when the cavity had a total length of 19.6(1) cm . In figure 2.9 multiple peaks of the same height and different widths are observed. When scanning with a very slow (1 Hz or lower) mechanical vibrations other than the mechanical resonance can be seen in the peaks [10]. Most likely combination of both of the mentioned effects is causing this distorted peak measurement.

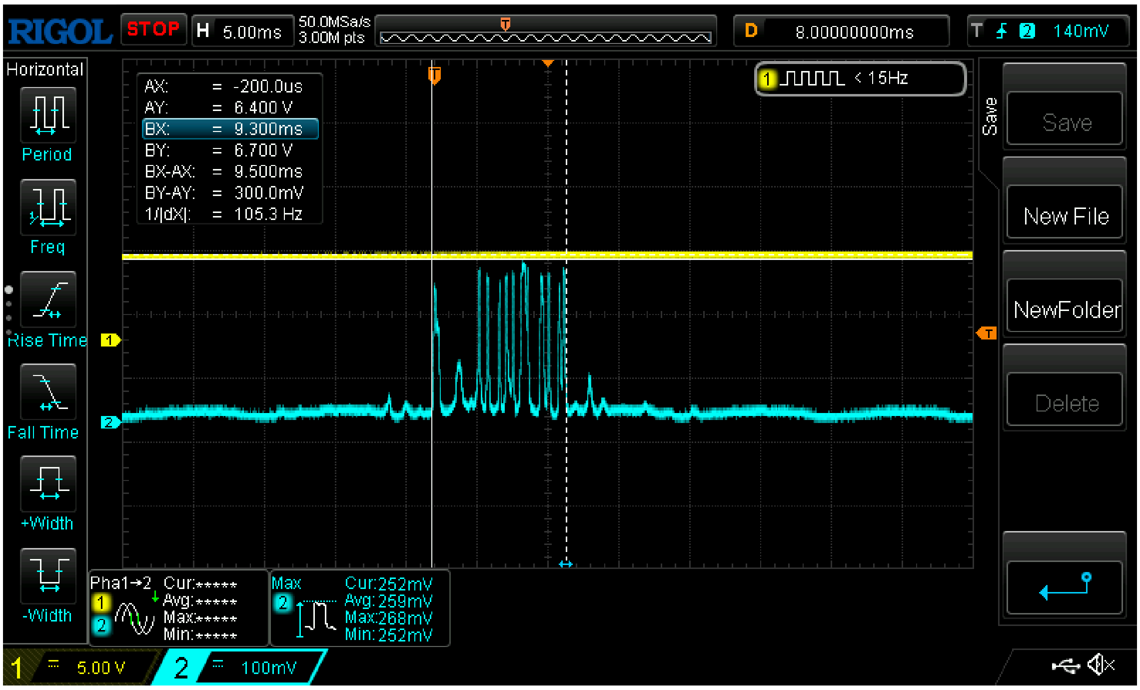

Figure 2.9: This screenshot shows degenerate modes in the cavity with the same mirrors as in the other measurements, but a total length of 19.6(1) cm instead of 18.6(1) cm.

When recording data of transmission peaks in a resolution lower than 1 MSample/s an asymmetric peak is observed. Similar behavior is observed in other cavities following the same design [2][11]. Fitting a Gaussian function to the signal is less precise than demonstrated in figures 2.5 and 2.7. An example of this is shown in figure 2.10.

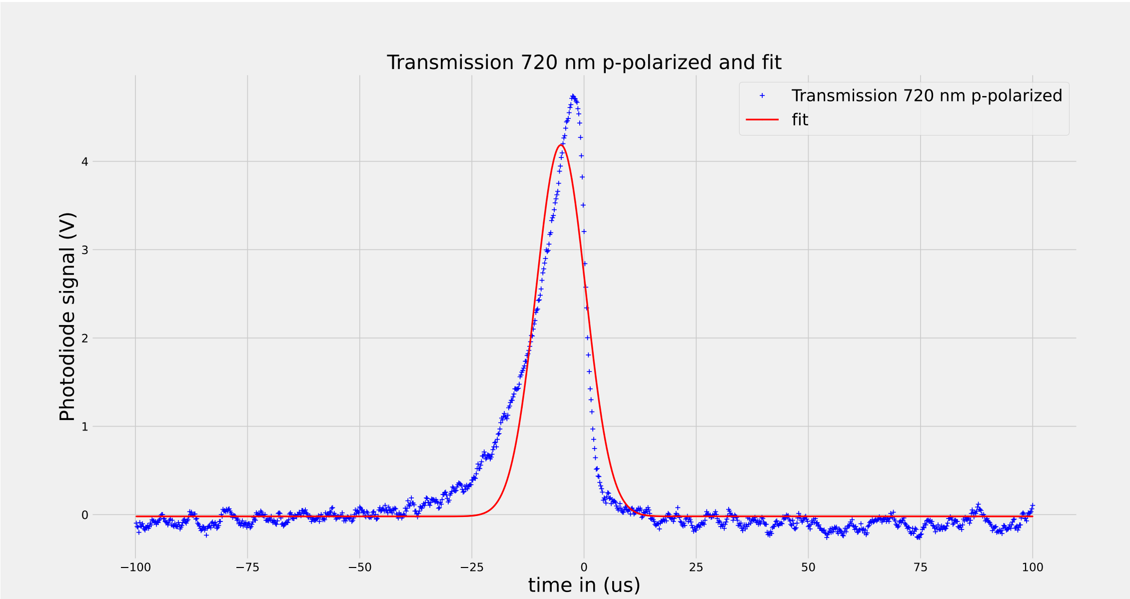

Figure 2.10: This picture shows an asymmetric transmission signal recorded at a wavelength of 720 nm and a scanning frequency of 50 Hz. This asymmetry is most likely caused by a lack of bandwidth where the incoming slope is not steep enough and the falling slope is a more accurate representation of the signal.

A possible cause of this behavior is found in bandwidth of the photodiodes at high gain settings. At higher gain settings the bandwidth of the photodiode decreases drastically. At highest gain setting the bandwidth is 5 kHz [12]. This decrease in bandwidth can result in the asymmetric peak shape.

2.2.6 Drift of the cavity

Since the cavity is neither temperature stabilized nor made out of ultra low expansion materials (ULE), it is subject to thermal drifts. Even small temperature fluctuations are noticeable since the resonance positions of the cavity is sensitive to length changes on the nanometer scale. To measure the thermal drift of the cavity the peak positions are recorded over different timescales, whilst the Piezo is scanning the cavity. The scan signal is a 50 Hz, 40 V triangular signal. By choosing this amplitude several peaks are visible in a single scan. This way more positions can be tracked. To record the curve with a high sample rate a Red Pitaya is used. This micro controller has two analog inputs and fast ADC. The sampling rate is controlled via the decimation factor. This factor controls the sampling rate as well as recorded time span per measurement instance.

For all the following measurements a decimation factor of 64 is chosen. This is equal to a sample rate of 1.953 MSamples/s and each measurement instance is recorded over a time of 8.389(1) ms [13]. Measuring the short time drift of the cavity a measurement of peak positions over two minutes is conducted. The peak positions are scaled using the previously calculated FSR of the cavity. A line is fitted to the peak positions to determine the drift, depicted in figure 2.11. The fit-function used is defined as:

$$f(x) = a \cdot x + b \tag{2.12}$$

From these fitted curve the average incline is determined. This is then used to measure the frequency drift over time. Over 120 seconds the cavity drifts 140(10) MHz. This is equal to a expansion of 55.5(1) nm. The thermal expansion coefficient α of 304 stainless steel is $\alpha = 17.4 \cdot 10^{-6} \frac{1}{K}$ at room temperature [14]. The temperature drift of the cavity is then calculated by

$$\Delta T = \frac{\Delta L}{\alpha \cdot l_0} = \frac{55.5(1)\ nm}{17.4 \cdot 10^{-6} \frac{1}{\mathrm{K}} \cdot 18.6(1)\ \mathrm{cm}} = 0.0174(1)\ \mathrm{K}\ [15] \tag{2.13}$$

Over the time of measurement the cavity heats up by 0.0174(1) K. This is equal to a shift of 8.15(0.1)GHz/K.

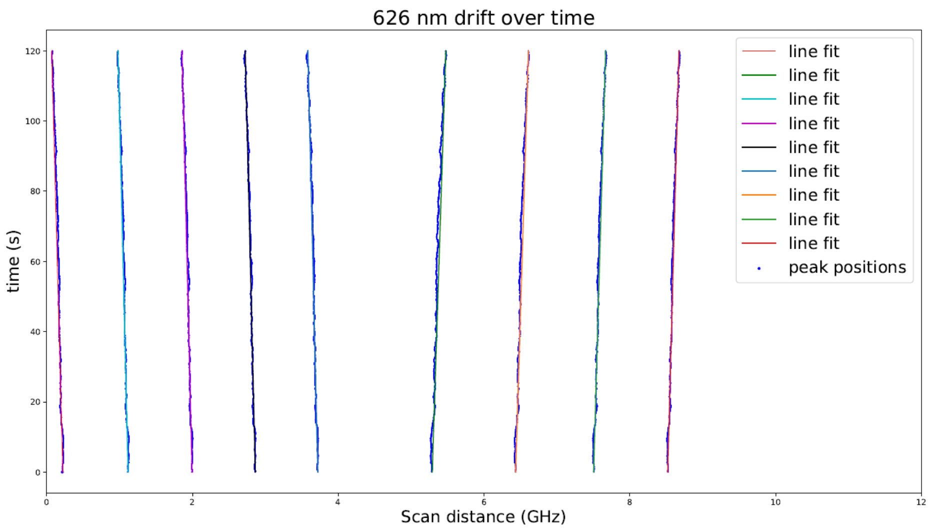

Figure 2.11: This plot shows the drift of peak positions over time due to thermal expansion. The direction of the peak movement changes in the middle of the measurement due to sign change of scan direction. The cavity expands by 55.5(1) nm over 120 seconds. This is equal to the cavity heating up by 0.0174(1) K.

In figure 2.11 the peak positions and their drift over a short period of time, including a line fit is shown. If the cavity does not drift at all the peak position stays the same. The change in direction of the peaks is caused by a direction change of the scan signal. For the first five peaks the cavity is getting shorter, due to the Piezo expanding. For last four peaks the the Piezo is retracting. Therefore the cavity is expanding. This can also be seen in the slope of the curves. The curve fitted to the peaks, where the cavity is getting smaller, has a greater slope than the one where the cavity is expanding. Furthermore, a change of peak distance is observable, translating to the change of expansion speed for the Piezo. This means that the Piezo expands slower than it contracts. Therefore the scale of the x-axis given in figure 2.11 is only correct for the first five peaks.
A drift measurement over longer periods of time is conducted as well. This measurement is shown in figure 2.12. Over the time of measurement the cavity's maximum drift is 5.48(0.1)GHz this is equal to a temperature fluctuation of 0.6(1) K. This comparable to the temperature drifts in our lab.

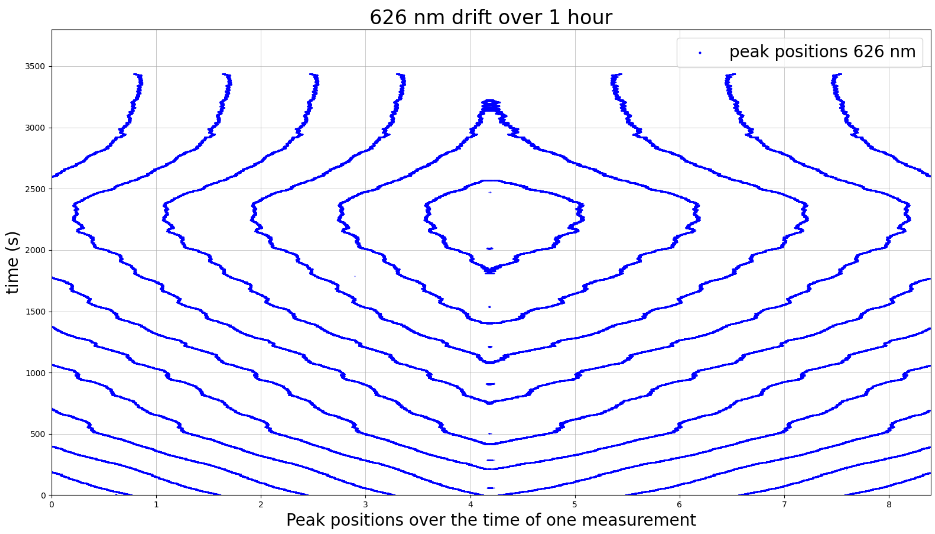

Figure 2.12: This figure shows the peak positions over an time of 1 hour. The maximum drift measured is 5.48 GHz. This is equal to a temperature drift of 0.67(2) K, which is comparable to temperature changes observed in the lab.

To verify that this drift is caused by temperature fluctuation as well as the direction of the temperature change seen in figure 2.11 another measurement is taken, where the cavity is suddenly heated. Here the cavity is heated by simply touching it with a hand after starting the measurement. The drift of the peak positions is depicted in figure 2.13. This measurement is taken at the same scan frequency and amplitude and is also triggered on the same scan slope as in the previous measurement.

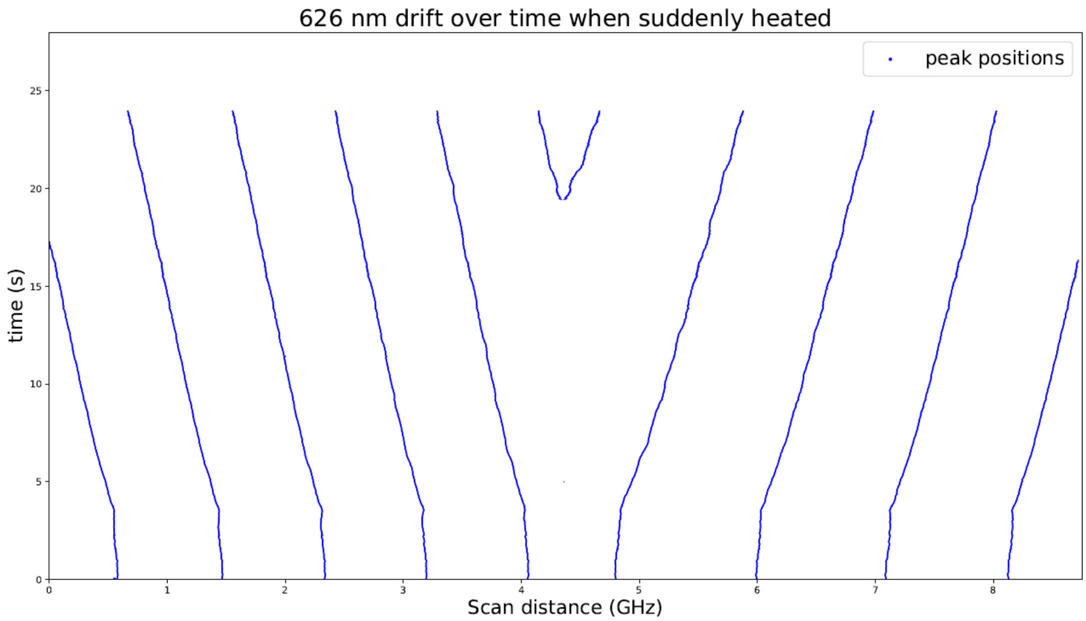

Figure 2.13: This figure depicts the peak positions over time. After a few seconds there is an abrupt change in the peak movement, due to heating the cavity with a hand.

In figure 2.13 the initial drift direction is the same as in figure 2.11. After 3 seconds the drift speed increases as the hand warms the cavity. Here the same behavior as in the previous drift measurement. The slope of the first five peaks is bigger than the slope of the last four peaks. This confirms the stated scan direction that the the cavity decreases in length before expanding again. In the heated measurement the drift increases that the cavity drifts more than a FSR over a short time span. This measurement also shows how susceptible the cavity is to small temperature fluctuations, emphasising the importance of a temperature stabilized environment for the cavity.

2.3 Summary

The transfer cavity described in this chapter scans two lasers, a 626 nm laser and a 720 nm laser. The 626 nm laser is locked to a ULE cavity and used as a reference to scan the drift of the 720 nm laser. To achieve this the cavity is build in a set-up depicted in figure 2.6.
With a total length of 18.6(1) cm the hemispheric cavity with a concave mirror curvature of 20 cm is stable under the stability condition given in (1.28).
Measuring the reflectivities of the plane and concave mirrors the finesse of the cavity is calculated. The measured reflectivities are listed in table 5.1. The finesse calculated from that is listed in the table 2.1. Here the large error is caused by the reflectivity measurement. To get more precise information on the cavity the finesse is also determined by measurements of the FWHM as well as the free spectral range (FSR) for each wavelength and polarization. Using this method the finesse of the cavity is measured again, resulting in a finesse with smaller error size. The finesse values are listed in table 5.2.
The length of the cavity is adapted to avoid degenerate modes and the sample rate is chosen as high as possible to avoid asymmetric peaks.
The frequency drift caused to thermal expansion is measured over short periods of time. Even for small temperature fluctuations in the material of the cavity the peaks drift noticeably. For a frequency shift of 140(10) MHz a temperature change of 0.0174(1) K is calculated. This is calculated to a frequency shift of 8.15(1)GHz/K

Since the finesse is high the slopes of the transmission peaks are too steep for a digital or analog PID controller to lock on. Therefore a side-of-fringe locking is not possible. Instead the cavity is used as a scanning cavity. This offers the advantage, that the FSR is no longer the limiting resolution factor, instead the cavity will be scanned continuously with the Piezo measuring the drift of the peaks in real time. Here the limiting factor is the length of the measurement. Using a Red Pitaya this can be reduced to $\approx 150\ \mu$s.

3 Characterization of the UV-system

3.1 Introduction

The dysprosium experiment in our lab uses a M-squared lasers system to create UV-light at 360 nm wavelength. The laser system consists of a Ti:Sa laser operating at 720 nm and a second harmonic generation cavity. The 720 nm light is used to characterize and in future stabilize the laser. The 360 nm light will be used to create the UV-optical lattice.
Previous studies showed that the frequency scan function of the M2 system has a non linearity [3]. This makes it challenging to conduct a sophisticated scan across the narrow UV-transitions of dysprosium.
To overcome these challenges the drift of the etalon-locked 720 nm laser compared to the 626 nm laser is measured as well as the scan function for the 720 nm laser.

3.2 Characterization of the 720 nm laser

Since the M-squared system is not locked to an external reference the laser it is subject to drift. In order to characterize those drifts both 626 nm and 720 nm light are coupled into the cavity and their realtive peak positions are recorded. The scan frequency of the Piezo is 50 Hz and has a scan voltage of 40 V_{PP}. Both 626 nm and 720 nm light are recorded, to account for the thermal drift of the cavity. If the 720 nm light doesn't drift the distance between the peaks of 626 nm and 720 nm should stay the same, since both experience the same thermal drift. A measurement of both wavelengths over ca 5 minutes is depicted in figure 3.1.

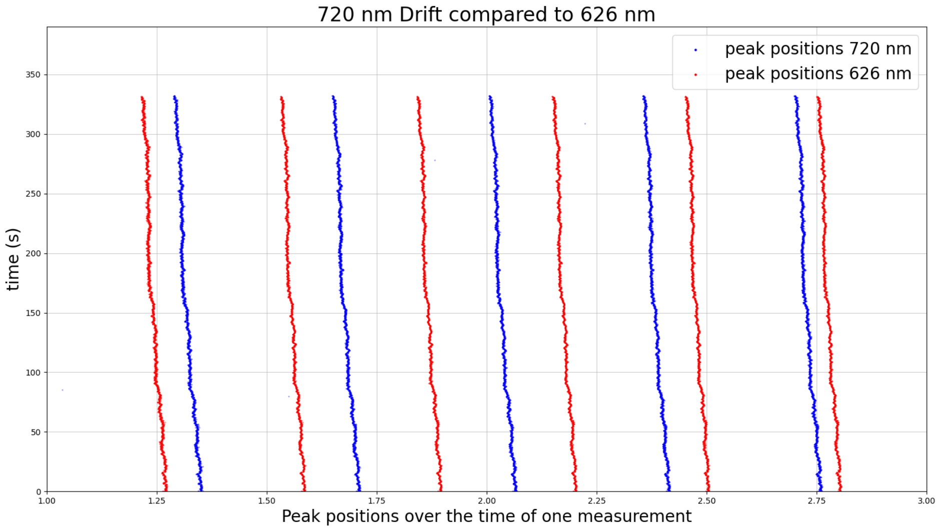

Figure 3.1: This figure shows the peak positions and the drift of 626 nm light and 720 nm light over ca 5 minutes. Both lasers are locked respectively, the 626 nm to an ULE cavity and the 720 nm laser to the internal etalon lock. Thermal drift is visible in both wavelengths due to the cavity heating up. The peaks of both wavelengths seem parallel, but with increasing time the distance between the two peaks changes slightly indicating a drift of the 720 nm light.

In figure 3.1 both 626 nm and 720 nm light experience drift in their positions due to temperature fluctuations. Over the measured time period of about 5 minutes the peaks seem parallel. At a closer look slight changes in distance in between the peaks can be observed. This behavior indicates a drift in frequency of the 720 nm light compared to the 626 nm light, which is locked by an ULE cavity. To analyze this behavior more in depth the measurement should be repeated over longer time spans compared with more sophisticated distance measurement in between the peaks.
The 720 nm laser system has an inbuilt frequency scan function. To characterize this scan function the 720 nm laser light is locked to the internal etalon and scanned over an internal resonator. The scan is controlled via the M-squared software. With a scan range of 1 GHz over a time of period duration of 10 seconds, the peak positions are recorded over multiple scans. For this measurement, the settings of the Piezo scanning the transfer cavity remains the same as described earlier, to measure the drift of the 720 nm system compared to the stabilized 626 nm light.
In figure 3.2 measurement of the peak positions for both 626 nm and 720 nm is shown over the duration of 8 frequency scan cycles.

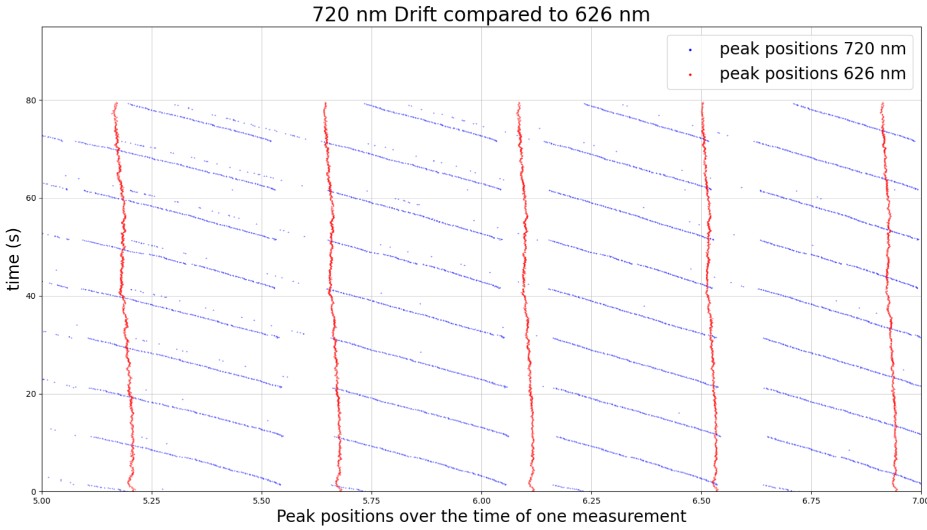

Figure 3.2: This figure depicts the peak positions for both 626 nm and 720 nm light, whilst the 720 nm light is being scanned over a range of supposedly 1 GHz. The calculated FSR of the cavity is 805.9(1)MHz. Using this information it is clearly visible that the scan does not cover the entire range of 1 GHz. The measured drift of the 720 nm light is about as big as a FSR, and therefore smaller than 1 GHz.

The shift in peak position measured for the 720 nm light covers about a FSR of the cavity. The calculated FSR is 805.9(1)MHz whereas the set scan distance of the 720 nm light is 1 GHz. Furthermore, the scan is not completely linear, fluctuations in peak positions can be seen over the cycle of a frequency scan. To characterize the non-linearity of the scan as well as a potential cause for the difference in set frequency scan length, further measurements are needed.
In both measurements the Piezo behavior is similar to the behavior observed in the drift measurements in section 2.2.6, where the Piezo expands slower than it contracts.

3.3 Summary

In this chapter the 720 nm laser-system is characterized regarding its drift behavior as well as the scan function. Over a short period of time the etalon locked 720 nm laser barely drifts. For longer time periods more measurements have to be taken.

When using the scan function of the laser a difference of almost 20% is measured regarding the set frequency scan distance and the measured scan distance. Furthermore a non-linearity in the scan frequency scan signal is detected. To characterize the non-linearity in the scan in more detail as well as find the origin of difference in frequency scan distance in the 720 nm system further measurement and testing is required.

4 Conclusion

Conclusion

In this Bachelor thesis an optical transfer cavity of the Tomschitz design is set-up and characterized. The cavity with a total length of L =18.6(1) cm is found to have a finesse $\mathcal{F}_{626}$ = 754(1) for p-polarized light and $\mathcal{F}_{626}$ =784(1) for s-polarized light. For 720 nm light the finesse is calculated to $\mathcal{F}_{720}$ = 679(1) for p-polarized light and $\mathcal{F}_{720}$ = 762(0.6) for s-polarized light. Furthermore the drift of the cavity is measured. The drift caused by temperature fluctuations of the cavity is a drift of 8.15(1)GHz/K.
To characterize the UV-laser system the drift relative to the locked 626 nm light is measured. Furthermore the frequency scan function is characterized. Over short periods of the the UV-laser, when locked to its internal etalon, is small compared to the thermal drift the cavity experiences. The scan function of the laser shows a non-linearity, as well as a difference in set frequency scan distance and measured frequency scan difference. This difference between set scan range and measured scan range can be as large as 20%.

Outlook

At the point of writing the thesis the measurements can only be evaluated after the measurement is completed. A goal for future application should be the instantaneous evaluation of the drift compared to the previous measurement to send instant feedback to the laser in order to stabilize the system over an indefinite amount of time. So far the transfer cavity is only used as a scanning cavity since the finesse is too high for side of fringe locking. To lock the cavity to the ULE stabilized 626 nm laser a PDH signal has to be created. Using some in house technology developed by our institute, the experimental control used for stabilization can be done using the Red Pitaya.
To characterize the UV-laser system a more sophisticated distance measurement between the stabilized 626 nm laser and the 720 nm laser is required. This would allow a precise study of the non linearity in the scan function as well as the drift of the 720 nm light. Furthermore, long time drift measurements of the 720 nm laser have to be taken, to see the effects more clearly.

Bibliography

[1] Tomas Maier. “Interactions in a Quantum Gas of Dysprosium Atoms”. University of Stuttgart, Oct. 2015.

[2] Christian Tomschitz. *A photoionization scheme to create cold ionic impurities from Rydberg atoms*. 2018.

[3] Viraatt Sai Vishwakarma’ ’Anasuri. “Shelving spectroscopy of a UV transition in Dysprosium atoms”. University of Stuttgart, Oct. 2019.

[4] Hecht. “hecht - optics 4th”. In: (2002).

[5] Torsten Fließbach. *Elektrodynamik*. Springer Berlin Heidelberg, 2022. DOI: 10.1007/978-3-662-64889-6.

[6] institution = University of Birmingham Miguel Dovale Álvarez city = Birmingham. “Springer Theses Recognizing Outstanding Ph.D. Research Optical Cavities for Optical Atomic Clocks, Atom Interferometry and Gravitational-Wave Detection”. 2019.

[7] Bahaa E. A. Saleh and Malvin Carl Teich. *Fundamentals of Photonics*. John Wiley Sons, Inc., Apr. 2003, pp. i–xix. DOI: 10.1002/0471213748.fmatter_indsub.

[8] ’https://commons.wikimedia.org/wiki/File:Laguerre-Gaussian$_{m}odes.png'$. “https://commons.w
Gaussian$_{m}odes.png, lastcalledDecember 1, 2022$”. In: (Feb. 2021).

[9] Francesco’ ’Pampaloni and Jörg’ ’Enderlein. “Gaussian, Hermite-Gaussian, and Laguerre-Gaussian beams: A primer”. In: (Oct. 2004).

[10] ’PI Ceramic GmbH’. “https://www.piceramic.de/de/produkte/piezokeramische-aktoren/linearaktoren/p-080-picma-stack-multilayer-ringaktor-100820specification last called December 1, 2022”. In: (2022).

[11] Simon’ ’Koppenhöfer. “Charakterisierung eines Lasersystems bei 420 nm zur Durchf uhrung eines Experiments mit einzelnen Photonen”. University of Stuttgart, Sept. 2020.

[12] ’THORLABS’. “https://www.thorlabs.com/$_{s}d.cfm?fileName = 13053-D04.pdfpartNumber$
$PDA36AlastcalledDecember 1, 2022$”. In: (2022).

[13] ’redpitaya’. “https://redpitaya.readthedocs.io/en/latest/appsFeatures/examples/acqRF-samp-and-dec.html last calledDecember 1, 2022”. In: (2022).

[14] 'Weltstahl.de'. "https://www.weltstahl.com/aisi-ss-304-edelstahl-datenblatt-werkstoff-18-8-rostfrei/". In: (2022).

[15] Wolfgang' 'Demtröder. *Experimentalphysik 1, Mechanik und Wärme*. 7th ed. Springer Spektrum Berlin.

Acknowledgments

Here I'd like to take a moment to show my gratitude to everyone that contributed to me being able to work on and finish this thesis.
First of all I'd like to thank Sean Graham who introduced me to the research topic of ultra cold quantum gases and inviting me to join the group here at the PI5.
Further I'd like to thank Prof. Dr. Tilman Pfau for giving me the opportunity to write my bachelor thesis at the PI5. Special thanks is also directed to everyone here at the Dysi-lab who were always there to anser my questions and taught me more than i could have ever imagined about the everyday procedures of experimental physics as well as on how to do proper scientific research. Especially to Paul Uerlings who proofread this thesis and always helped me out with his expertise and experience.
This section wouldn't be complete without me thanking all the friends that I made over my bachelor studies and those who where there even before I started studying physics. Without all of you I wouldn't even have been able to make it to the point where I can even apply to work on a bachelor thesis. Here special thanks goes to my brother Patrick and my friend Mofi who were always very patient, when explaining the documentations and technical terms of various programming documentations to me.
Last but not least I have to thank my family. Namely my parents, my brother and Isabella for always supporting and motivation me in my studies, to continue even in bleakest moments.
Without all of you this wouldn't have been possible.
THANK YOU.

5 Appendix

Reflectivity measurements

This table contains the measured reflectivites used to calculate the finesse of the cavity in table 2.1

mirror	wavelength in nm	polarisation	relfectivity in %
Edmund optics #87-368	626	p	99.80(5)
Edmund optics #87-368	626	s	99.94(5)
Edmund optics #87-368	720	p	99.94(5)
Edmund optics #87-368	720	s	99.94(5)
CM254-100-E02	626	p	99.98(5)
CM254-100-E02	626	s	99.96(5)
CM254-100-E02	720	p	99.99(5)
CM254-100-E02	720	s	99.96(5)

Table 5.1: This table contains the measured reflectivites used to calculate the finesse of the cavity in table 2.1

Cavity characterization

Table 5.2 shows all measured and calculated values for the finesse, the FWHM and the FSR for 626 nm and 720 nm light with both p- and s-polarization.

Table 5.2: This table lists the measured FSR, FWHM and finesse measured for 626 nm and 720 nm light for both s- and p-polarization.

Light	FSR in ms	FWHM in μs	Finesse
626 nm p-pol.	2.372(1)	3.143(1)	754(1)
626 nm s-pol.	2.397(1)	3.022(1)	784(1)
720 nm p-pol.	2.483(1)	3.653(1)	679(1)
720 nm s-pol.	2.514(1)	3.129(1)	762(1)

Technical drawings for custom parts used in this thesis

Technical drawings of the spacer and the Piezo holder are shown in figure 5.1 and 5.2 respectively.

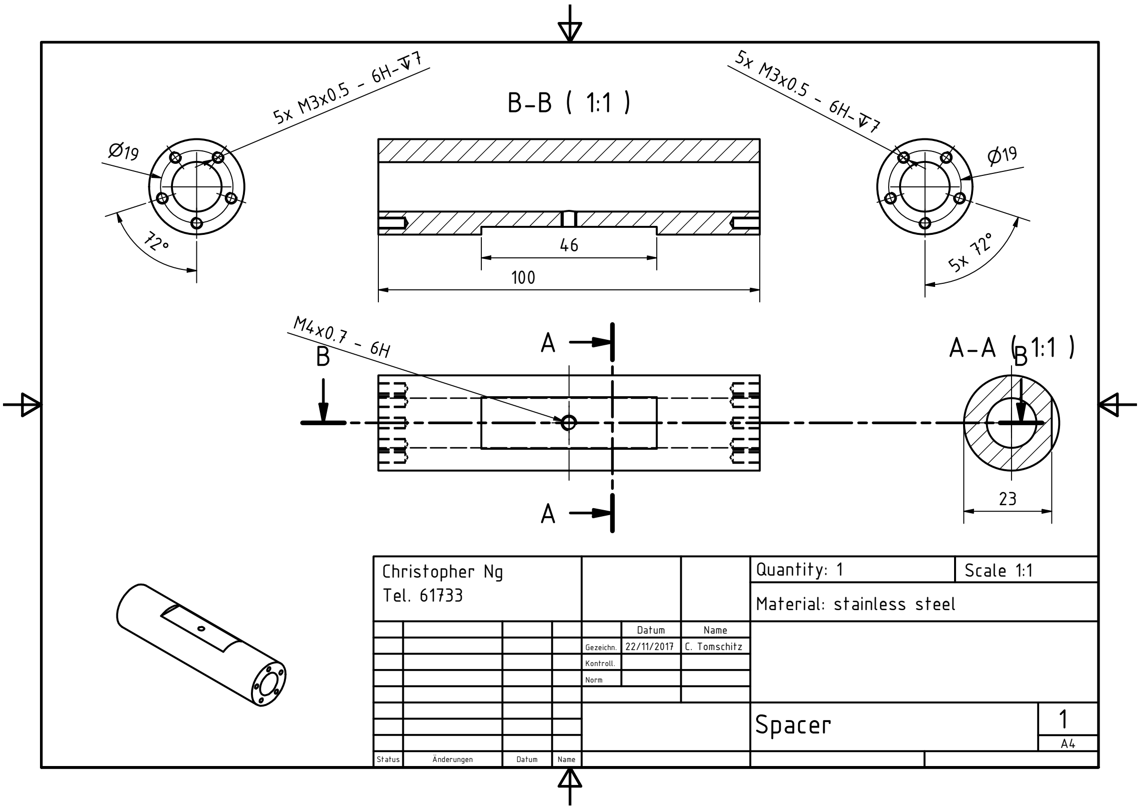

Figure 5.1: This figure shows the inventor sketch for the spacer used in the experiment.

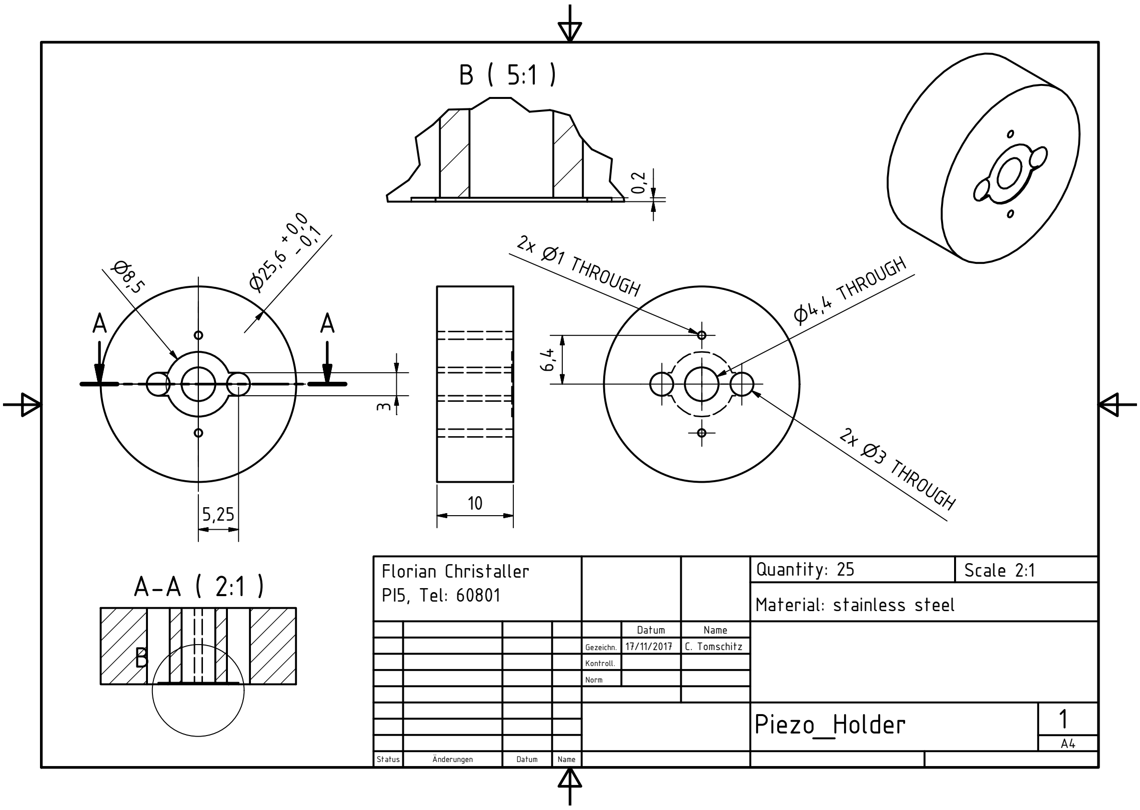

Figure 5.2: This figure shows the inventor sketch for the Piezo holder used in the experiment.